Journal of Alloys and Compounds 697 (2017) 90–95

Contents lists available at ScienceDirect

Journal of Alloys and Compounds

journal homepage: http://www.elsevier.com/locate/jalcom

Influence of titanium doping on the Raman spectra of nanocrystalline $ZnAl_2O_4$

Vlasta Mohaček-Grošev [a, b], Martina Vrankić [a, b, *], Aleksandar Maksimović [a, b], Vilko Mandić [b]

[a] Center of Excellence for Advanced Materials and Sensing Devices, Ruđer Bošković Institute, Bijenička 54, 10000 Zagreb, Croatia
[b] Division of Materials Physics, Ruđer Boskovic Institute, Bijenicka 54, 10000 Zagreb, Croatia

ARTICLE INFO

Article history:
Received 18 October 2016
Received in revised form
2 December 2016
Accepted 9 December 2016
Available online 11 December 2016

Keywords:
Inorganic materials
Optical materials
Preferential site ordering
Optical properties
Phonons
Optical spectroscopy

ABSTRACT

The local structural changes within the normal spinel structure of a $ZnAl_2O_4$ host caused by the titanium incorporation as studied by the Raman spectroscopy and computationally using the density functional theory have been analyzed. The lattice dynamics calculation of the $ZnAl_2O_4$ phonons were performed within the density functional theory for the 3D periodic crystal structures. Band structure calculations by the grid-based PAW method predicted a direct band gap in the pure $ZnAl_2O_4$ sample to be 4.732 eV, while doping with Ti^{4+} produced a density of states in the middle of the gap. The lattice dynamics calculations using Gaussian-type wavefunctions as basis set and a local density approximation gave a good agreement between observed and predicted Raman bands. Doping with Ti^{4+} causes the infrared active T_{1u} phonons as well as the inactive phonons (T_{1g}, A_{2u}, E_u and T_{2u} symmetries) to appear in the Raman spectra and breaking of the symmetry selection rules.

1. Introduction

Because of its stable crystal structure under high- and low-energetic ion bombardment, zinc aluminate, $ZnAl_2O_4$, has been considered as an appropriate material for a storage of nuclear waste [1]. Naturally occurring $ZnAl_2O_4$ mineral called gahnite can be found as an opaque, 94–98.7 mol % pure single crystal whose composition is very close to the stoichiometric formula [2]. Synthetic zinc aluminate with a large surface area is used as a catalyst [3], while its high-temperature stability makes it suitable as a ceramic material [4]. Furthermore, it is a semiconductor with a wide energy gap of ~3.9 eV, large absorbance in the UV region and transparency for wavelengths greater than 320 nm, which makes it applicable for various ultraviolet photoelectronic devices [5]. When doped with Co^{2+}, Mn^{2+} or rare-earth cations, it exhibits luminescence and can be used as a cathodoluminescent material [6]. In particular, $ZnAl_2O_4$ exhibits blue photoluminescence on doping with Eu^{3+} or Ti^{4+} cations which makes this material potentially suitable for solid state lasers [7–9].

Gahnite, $ZnAl_2O_4$, is an oxide of the spinel type, described with a general formula AB_2O_4, having a cubic close-packed crystal structure belonging to the $Fd\bar{3}m$ space group [10,11]. The unit cell contains 32 oxygen anions O^{2-} in the ccp lattice, 8 tetrahedral sites occupied by the divalent cations A^{2+} and 16 octahedral sites occupied by the trivalent B^{3+} cations. In the normal spinel structure divalent cations occupy tetrahedral sites with the fourfold coordination, while trivalent cations enter the octahedral sites having the six-fold coordination.

In the following, local structural changes caused by Ti^{4+} as studied by Raman spectroscopy and computationally using the density functional theory shall be discussed, regarding the hypothesis of Dereń et al. [9] that the partial inversion occurs in the doped gahnite structure. We shall demonstrate a good agreement between theoretical values of phonon positions and observed ones for the pure gahnite. Although one expects a breaking of the symmetry selection rules on doping, the intensity of the new Raman bands that emerge was unexpectedly high for a low level of doping undertaken. Furthermore, to test whether the bands observed in the Raman spectra were true Raman bands, we undertook the Raman spectroscopy measurements with two different

* Corresponding author. Ruđer Boskovic Institute, Bijenicka 54, 10000 Zagreb, Croatia.
E-mail addresses: mohacek@irb.hr (V. Mohaček-Grošev), mvrankic@irb.hr (M. Vrankić), Aleksandar.Maksimovic@irb.hr (A. Maksimović), Vilko.Mandic@irb.hr (V. Mandić).

http://dx.doi.org/10.1016/j.jallcom.2016.12.116
0925-8388/

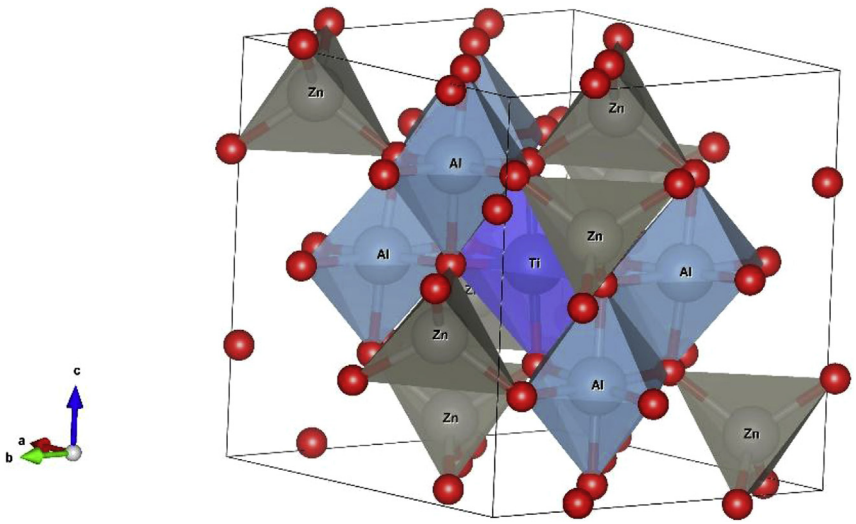

Fig. 1. Titanium doped $ZnAl_2O_4$ at the lowest titanium concentration: two Al atoms were replaced with one Ti and one Zn atom. In the conventional unit cell there are altogether 56 atoms present.

excitation lines, finding very similar spectra. The only difference concerned one ZnO band at 439 cm^{-1}, which was comparable to the gahnite phonons when green excitation was used. On doping, new phonon bands that emerge in the Raman spectra of a Ti^{4+}-doped $ZnAl_2O_4$ host coincide with the phonons present in the infrared spectra, or with the calculated values for the inactive phonons of a pure gahnite. Herein, we shall argue that these facts are in an accordance with the normal spinel structure in a Ti^{4+}-doped gahnite.

2. Experimental

2.1. Sample preparation

All the reagents were used as supplied with an analytical grade without any further purification. Powder samples of pure $ZnAl_2O_4$ and ones doped with titanium in the amounts of 1.8, 3.8, 5.4, and 11.6 at.% (hereinafter denoted as S0, S1, S2, S3 and S4, respectively) were prepared using a sol–gel technique [8]. The obtained samples were grinded to fine powders, heated up to 800 °C in the furnace with static air at a heating rate of 10 °C/min, and calcined at that temperature for 2 h. Afterwards they were slowly cooled to a room temperature (RT) in the furnace. All prepared samples were of a white color.

2.2. Raman and infrared spectroscopy

The Raman spectra of powder samples were recorded using two different excitations. The spectra obtained with a green laser line 514.5 nm of the COHERENT INNOVA 400 laser were recorded under the microscope of the T64000 HORIBA JobinYvon Raman spectrometer in the single mode. To check whether all of the bands were indeed Raman and not luminescence bands, the spectra of all samples were also obtained using the 785 nm near infrared laser with a Renishaw INVIA spectrometer. An excellent agreement between two Raman spectra was found, with the sole exception of the ZnO phonon band located at 439 cm^{-1}. This phonon band was observed only with a green excitation and is a result of a known

Table 1
Comparison of the observed and calculated phonons for gahnite $ZnAl_2O_4$ (cm^{-1}). Raman active modes belong to A_g, E_g and T_{2g} irreducible representations. Calculated values were obtained with the CRYSTAL09 program [12].

$ZnAl_2O_4$ $Fd\bar{3}m$ symmetry	Raman modes		Infrared modes		Inactive
	Observed	Calculated	Observed	Calculated	calculated
A_{1g}	758[a]	779			
A_{2u}					759
A_{2u}					691
T_{1u}			684	677	
T_{2g}	659	663			
E_u					582
T_{1u}			574	542	
T_{2g}	509	511			
T_{1u}			510	483	
T_{2u}					462
E_g	420	412			
E_u					400
T_{1g}					351
T_{2u}					251
T_{1u}			220–231[a]	212	
T_{2g}	196[a]	194			
T_{1u}					

[a] Data cited from Chopelas and Hofmeister [27].

green photoluminescence in that material.

The infrared spectra were recorded in the 4000–350 cm^{-1} region with the samples as KBr pellets by using a Bruker Alpha FTIR spectrometer.

3. Theory/calculation

The lattice dynamics calculations of the $ZnAl_2O_4$ phonons were performed within the density functional theory as implemented in the CRYSTAL09 program [12] for the 3D periodic crystal structures. The starting gahnite crystal structure belongs to the cubic $Fd\bar{3}m$ space group with the unit cell parameter, $a = 8.0854$ Å [8]. The fractional positions of oxygen atoms were $x = y = z = 0.2644$, in an accordance with the preparation temperature of 800 °C reported earlier by O'Neill and Dollase [10]. The atomic positions were optimized by using the Vosko-Wilk-Nusair parametrization of the correlation part [13] and a local density approximation for the exchange part of the Hamiltonian [14]. All frequencies were calculated within the harmonic approximation at the Γ point of the Brillouin zone. The zinc and aluminum basis sets were the triple zeta valence functions of Peintinger et al. [15], while the oxygen basis was that of Gatti et al. [16]. For a model of a Ti-doped $ZnAl_2O_4$ we used a conventional unit cell containing 56 atoms where two Al atoms were replaced with one Ti and one Zn atom in such a way that a single Al atom is placed between them. The 2/56 ratio was chosen to correspond to the sample S1, containing 1.8 at.% Ti^{4+} [8]. This conventional unit cell is represented in Fig. 1. All calculations were done on the HP Z640 workstation using eight processors. The geometry optimization of the Ti^{4+}-doped $ZnAl_2O_4$ structure lasted three and a half days, while the phonon calculation took nine days.

In order to obtain a density of states, quantum mechanical calculations were carried out within the density functional theory [17–19] using the real space grid-based projected augmented wave (GPAW) code which implements the projected augmented wave (PAW) method [20]. The meta-GGA calculations were performed using standard GPAW PBE pseudopotentials, within the atomistic simulation environment (ASE) interface connected with the GPAW code [21]. The Broyden–Fletcher–Goldfarb–Shanno (BFGS) local optimization algorithm [22] available in the ASE, was used to iteratively find the structural energy minimum, where all atomic forces are below 0.05 eV/Å. The accuracy of a real-space representation was controlled with the grid spacing. The default value of 0.2 Å was chosen since smaller values took too much time although the precision was increased. The Brillouin-zone was sampled with a regular grid of $4 \times 4 \times 4$ k-points with the Monkhorst-Pack scheme.

4. Results

Two formula units of a $ZnAl_2O_4$ in the primitive cell of the $Fd\bar{3}m$ space group contain fourteen atoms having 42 spatial degrees of freedom and span the following irreducible representations [23,24] given by the following equation:

$$\Gamma = A_{1g} \oplus E_g \oplus T_{1g} \oplus 3T_{2g} \oplus 2A_{2u} \oplus 2E_u \oplus 5\,T_{1u} \oplus 2T_{2u}. \quad (1)$$

The modes A_{1g}, E_g and T_{2g} are Raman active, while T_{1u} are infrared active. One T_{1u} mode corresponds to triply degenerate acoustic phonon of zero frequency at the Γ point. In Table 1 a comparison of the observed and calculated phonons of a pure nanocrystalline $ZnAl_2O_4$ sample is given. It is well known that the infrared spectra of spinels are characterized by absorption bands in the range 400–700 cm^{-1} [25,26]. Thereby, a relatively strong absorption band corresponding to the stretching vibration of the atom in the tetrahedral oxygen environment was located at ~660 cm^{-1} (Fig. 4). On the other hand, the strong band observed at

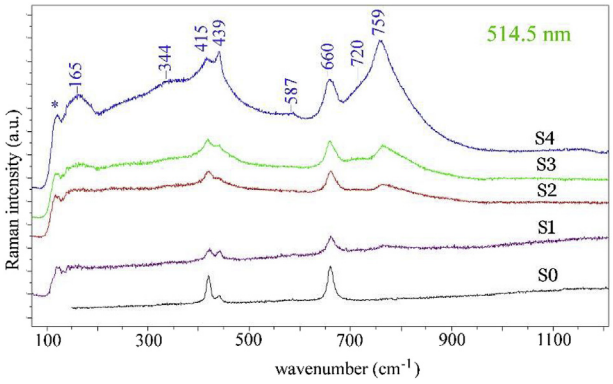

Fig. 2. Raman spectrum of the sample S0 compared with the Raman spectra of samples S1, S2, S3 and S4 obtained by using a green laser line at 514.5 nm. Peak denoted with asterisk is an artifact due to the notch filter used. The band at 439 cm^{-1} is a ZnO impurity phonon band. (For interpretation of the references to colour in this figure legend, the reader is referred to the web version of this article.)

~550 cm^{-1} is characteristic for the stretching vibrations of the atom in the octahedral oxygen environment. Raman spectra obtained with 514.5 nm and 785 nm are displayed in Figs. 2 and 3, respectively. Two strongest bands at 420 and 659 cm^{-1} correspond to the E_g and T_{2g} modes, while a weak band at 509 cm^{-1} is assigned to the T_{2g} mode. Two Raman bands at 196 and 758 cm^{-1} observed by Chopelas and Hofmeister [27] were not observed, while a good correspondence with the observed infrared modes from this work was established (Fig. 4). Several inactive phonons are predicted at 251 (T_{2u}), 351 (T_{2u}), 400 (E_u), 462 (T_{2u}), 582 (E_u), 691 (A_{2u}) and 759 cm^{-1} (A_{2u}). These values do not take into account the LO-TO splitting which occurs in the Raman and infrared spectra of oriented single crystals in compounds where charged ions vibrate. As explained by Pandey et al. [28,29] the degeneracy of the transverse optical (TO) and longitudinal optical (LO) modes is broken due to the electric field that is generated during vibration. A correction term to the dynamical matrix element can be calculated if the Born effective charges are known, and the calculated TO and LO values are compared to the experimental ones. Since we investigated powder samples and not single crystals, and the symmetry has disappeared on doping anyway, we did not calculate the magnitude of the TO-LO splitting.

Doping with Ti^{4+} causes the appearance of additional bands located at 165, 258, 344, 587, 720 and 759 cm^{-1}, as well as a rise of the ZnO phonon at 439 cm^{-1} (Figs. 2 and 3), respectively. Namely,

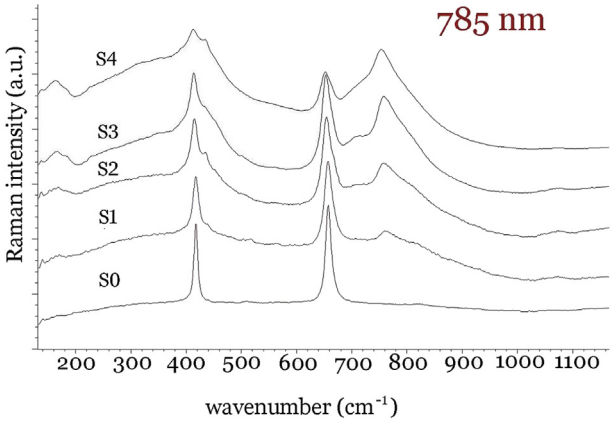

Fig. 3. Raman spectrum of the sample S0 compared with the Raman spectra of samples S1, S2, S3 and S4 obtained using a near infrared laser line at 785 nm.

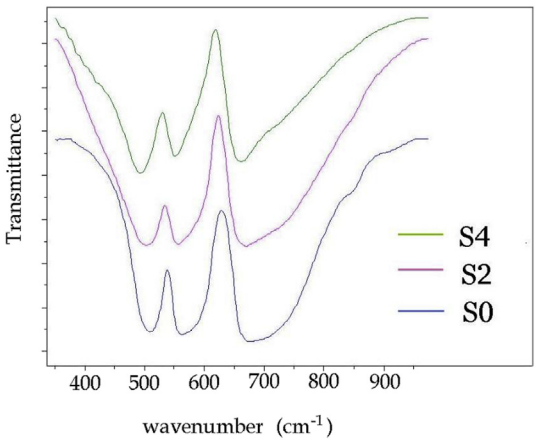

Fig. 4. Infrared spectra of samples S0, S2 and S4.

as the band at 759 cm^{-1} in particular seems to be sensitive to titanium doping, the corresponding phonon was looked into more carefully by using the MOLDRAW program [30]. In an agreement with the previous reports on the Raman spectra of a $ZnAl_2O_4$ spinel [31], motion of oxygen atoms dominates in this mode in the pure compound. On doping with titanium, however, thirteen phonons appear in the range 730–795 cm^{-1} which together produce two prominent maxima at 740 and 788 cm^{-1} in the Raman spectrum (Fig. 5). The list of all calculated phonons for the sample S1 is given in the Supplementary Table S1. Since the total density of states (DOS), obtained from the non-spin-polarized calculations can be used to visually estimate a band gap, we employed the ASE function which gives the minimum value between difference of the valence and conduction band for the direct gap equal to 4.732 eV. The DOS calculation indicated a new peak in the middle of the above gap (Fig. 6). The titanium atoms contributed to the peak in the gap – see Supplementary Fig. S3 for the contributions of different atomic species and their orbital projected density of states PDOS.

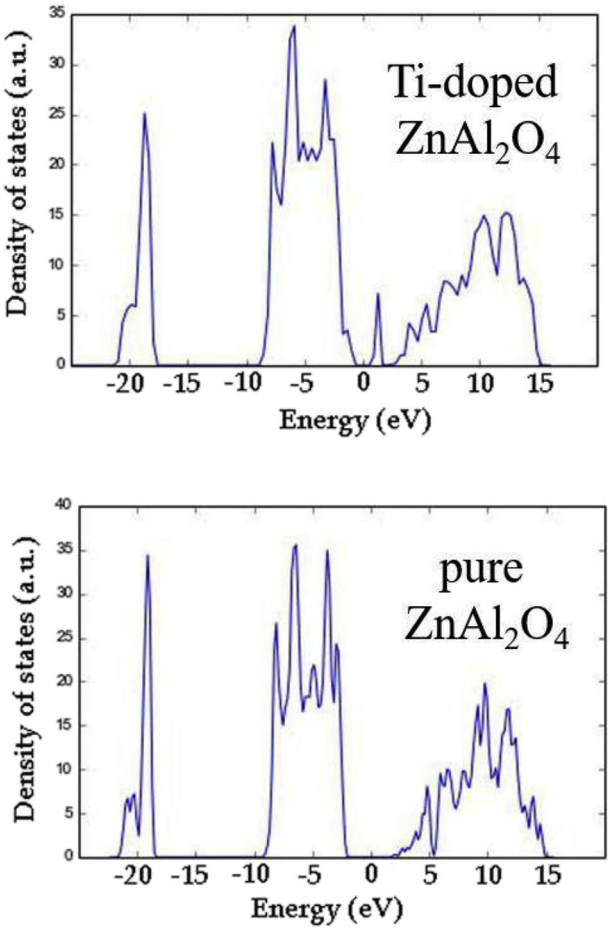

Fig. 6. Comparison of the calculated density of states for titanium doped and pure $ZnAl_2O_4$ host. The band gap is found to be 4.732 eV in the pure compound, while new states merge in the gap on doping.

5. Discussion

The previous band structure calculations on the $ZnAl_2O_4$ were reported by Sampath et al. [32], Khenata et al. [33,34], Dixit et al. [35,36], Fang et al. [37], and Lopéz-Moreno et al. [38]. Of these, only Fang and Lopéz-Moreno groups carried out the lattice dynamics calculations of phonons. Namely, Fang et al. compared the calculated values with the phonon density of states obtained by the neutron scattering, while Lopéz-Moreno et al. reported a first-principles density functional study of the vibrational properties of the pure $ZnAl_2O_4$ compound [37,38]. In the reported high pressure Raman spectra a great overlap of gahnite bands with bands of methanol, ethanol and ruby used in high pressure Raman cell was observed, thus complicating the comparison with the calculated values [38]. Another study concentrating on the defects important for the conducting properties was done by Dixit et al. [36]. Namely, the band gap of a $ZnAl_2O_4$ was calculated using the HSE06 functional with the 37.5% mixing of a Hartree-Fock exchange and equal to 6.63 eV being very close to the best theoretical value of 6.55 eV. However, according to Dixit et al. the real experimental value must be higher than the reported one of 3.9 eV [5]. Furthermore, all electron calculations with an augmented plane wave as implemented in the WIEN2k code gave the band gap values close to 4.28 eV [33] or 5.2 eV for pure, and 5 eV for Ti-doped $ZnAl_2O_4$ [9]. Our choice of the most appropriate functional was based on a comparison of the phonons positions calculated by using the Vosko-Wilk-Nusair [13], Perdew-Becke [18,19], and Perdew-Wang generalized gradient approximation [39]. The Vosko-Wilk-Nusair (VWN) functional gave the best agreement with the observed phonons' positions, like A_g mode at 779 cm^{-1} compared to an experimental value of 758 cm^{-1}, whereas other two gave the values above 800 cm^{-1}. Also, the T_{2g} mode observed at 659 cm^{-1} was predicted at 663 cm^{-1} using the VWN, but was calculated to be at

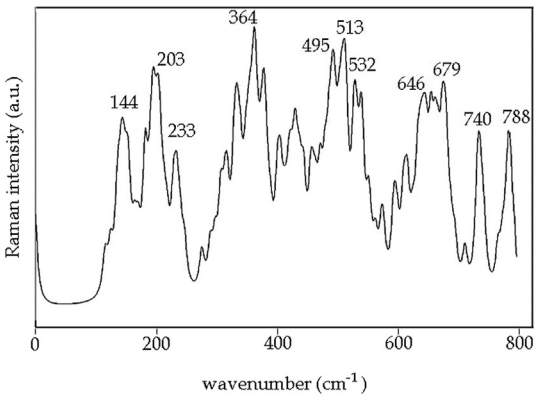

Fig. 5. Calculated Raman spectrum of titanium doped $ZnAl_2O_4$. For several prominent bands the wave numbers above the bands are indicated (cm^{-1}). Two Al atoms were replaced with one Ti and one Zn atom in the conventional unit cell with 56 atoms.

681 cm^{-1} using the PWGGA, or much lower at 601 cm^{-1} using the PBE (see Supplementary Table S2).

Comparing our optimized values of a cell parameter $a = 7.9639$ Å and an internal parameter $u = 0.2637$ with the experimental ones reported by Vrankić et al. ($a = 8.0854$ Å and $u = 0.2644$) [8] we find a good agreement. The value of a direct band gap which we obtained, 4.732 eV, is higher than the experimental value of 3.9 eV reported by Sampath et al. [5]. But still, this overestimate is found by other authors as well [9,33,36].

Nanocrystalline nature of the pure and titanium doped samples becomes evident through the bandwidth of the observed Raman transitions. In the study of the effect of a nanocrystallinity in the pollycrystalline TiO_2, Swamy et al. reported the gradual increase of the bandwidth of Raman bands as particle diminish in size [40]. At the same time, the number of observed bands does not change at the ambient pressure. Our main goal was however to assign the Raman bands in nanocrystalline $ZnAl_2O_4$ sample and study the effect of Ti doping on Raman spectra. We found a good agreement between observed Raman bands in pure nanocrystalline $ZnAl_2O_4$ compound with those for single crystal gahnite reported by Chopelas and Hofmeister [27], since two strongest bands at 415 and 660 cm^{-1} dominate the Raman spectrum. Furthermore, the Raman bands reported here for pure and doped $ZnAl_2O_4$ compound are indeed broader than those observed in the single crystal reported by Chopelas and Hofmeister [27], but at the same time their positions correspond well with values calculated for an infinite periodic crystal (Table 1). An additional weak band at 439 cm^{-1} is due is due to presence of a ZnO phase in the Ti^{4+}-doped $ZnAl_2O_4$ samples. Namely, in the previous publication reported by Vrankić et al., it was established that in the Ti-doped samples the occupancy of Al atoms on ^{VI}B sites changes from 100% in pure $ZnAl_2O_4$ towards 76.8% in maximally doped samples, while Zn atoms gain occupancy on the same sites [8]. The simultaneous appearance of a ZnO Raman band located at 439 cm^{-1} indicates that thermodynamic conditions during the synthesis were a Zn-rich [36]. Taking this into account, in the model presented here, the two Al atoms were removed and one Ti and one Zn atom were substituted instead. Considering the electron-phonon interaction which is the underlying cause of the polaron formation, we may take an example of a TiO_2 compound in which the conducting electrons localize at Ti^{4+} sites to form Ti^{3+} [41]. The activation energy they found for a polaron hopping is ~0.3 eV parallel to *c* direction in rutile, while for other directions it was order of magnitude smaller. Polaron defects of the Ti^{3+} type are much less abundant than Ti^{4+} cations in the Ti-doped $ZnAl_2O_4$ [8], therefore this type of defects is considered not to be relevant. The optical conductivity of superconducting oxides is known to display the broad maxima in the range 0.2–0.7 eV, which are measured by an infrared spectroscopy [42]. According to Emin [43] the polarons in ionic compounds can involve displacement of atoms' equilibrium positions over several elementary cells. The energies of these polarons are large, typically several electron volts, and the bound polaron states would completely distort the observed phonon spectra. However, the broad band shapes in the Raman and infrared spectra of a nanocrystalline Ti-doped gahnite are caused by the nanosized nature of the samples. The number of observed Raman phonons does not change on doping, but the symmetry of forbidden bands becomes visible.

Doping with Ti^{4+} causes the infrared active T_{1u} phonons as well as the inactive phonons (T_{1g}, A_{2u}, E_u and T_{2u} symmetries) to appear in the Raman spectra (Figs. 2 and 3). Specifically, a broad shoulder located at 258 cm^{-1} corresponds to T_{1u} and T_{2u} phonons calculated at 212 and 251 cm^{-1}, band at 344 cm^{-1} corresponds to T_{1g} phonon calculated at 351 cm^{-1}, band at 587 cm^{-1} corresponds to E_u phonon calculated at 582 cm^{-1}, shoulder at 720 cm^{-1} corresponds to A_{2u} phonon calculated to lie at 691 cm^{-1}, while strong band at 759 cm^{-1} overlapping the A_{1g} gahnite mode corresponds to A_{2u} mode calculated at 759 cm^{-1} (compare Fig. 2 and Table 1), respectively. As all of these emerging bands are also present in the Raman spectra obtained with the 785 nm excitation (Fig. 3), they can not be assigned to the luminescent bands of trace impurities such as those observed in the Al_2O_3 with the 193 ppm Fe [44].

The infrared bands of doped powder samples are very broad (Fig. 4) and their maxima are shifted from the TO and LO modes obtained by reflection on a single crystal $ZnAl_2O_4$. Namely, the observed broad maxima at 510, 574 and a very large asymmetric band at 684 cm^{-1} are shifted from the TO-LO modes located at 440–532.7 cm^{-1}, 542.9–608.4 cm^{-1} and 640.6–787.3 cm^{-1} (all T_{1u}), respectively [27]. In particular, Dereń et al. suggested the hypothesis that the intensity increase of the infrared band at 217 cm^{-1} and a shoulder at ~800 cm^{-1} in a Ti^{4+}-doped $ZnAl_2O_4$ occurs on behalf of the partial inverse spinel ordering [9]. As discussed by D'Ippolito et al. [31] an inversion in the aluminate spinels might be indicated via an additional shoulder on the Raman E_g mode at 420 cm^{-1}. However, in our Raman spectra no other bands are observed in the vicinity of the E_g transition except the ZnO band at 439 cm^{-1} (see Supplementary Fig. S2).

Doping with titanium causes the significant spectral changes in the Raman spectra and breaking of symmetry selection rules. Based on a crystallographic analysis presented earlier [8] where no inverse spinel ordering was found, we conclude that the replacement of aluminum atoms by titanium and zinc atoms in the Ti-doped $ZnAl_2O_4$ samples causes the loss of the symmetry and consequently the Raman spectral activity of all phonon transitions present. Obtained theoretical calculations enhanced and expanded the already documented state-of-the-art puzzle [8] and thus a shed a light on the optical performance of the Ti^{4+}-doped $ZnAl_2O_4$ compound.

6. Conclusion

The Raman spectroscopic analysis and density functional theory computational methods were applied in the study of a nanocrystalline Ti^{4+}-doped $ZnAl_2O_4$ in order to find more information on local (dis)order. Band structure calculations by the grid-based PAW method predicted a direct band gap in the pure $ZnAl_2O_4$ sample to be 4.732 eV, while doping with titanium produced the density of states in the middle of the gap reducing its value to 2.4 eV. Former explains the origin of the blue luminescence in this material. The lattice dynamics calculations performed with the CRYSTAL09 program using Gaussian-type wavefunctions as basis set and a local density approximation gave a good agreement between observed and predicted Raman bands. On titanium doping, one observes both Raman allowed as well as the $ZnAl_2O_4$ infrared active and inactive phonons in Raman spectra.

Acknowledgment

We gratefully acknowledge the help of Mr. Josef Sedlmeier from the RENISHAW Company for acquisition of Raman spectra with the 785 nm excitation.

Appendix A. Supplementary data

Supplementary data related to this article can be found at http://dx.doi.org/10.1016/j.jallcom.2016.12.116.

References

[1] G. Baldinozzi, D. Simeone, D. Gosset, S. Surblé, L. Mazerollés, L. Thomé, Nucl. Inst. Methods Phys. Res. B 266 (2008) 2848–2853.

[2] V. D'Ippolito, G.B. Andreozzi, F. Bosi, U. Hålenius, L. Mantovani, D. Bersani, R.A. Fregola, Mineral. Mag. 77 (2013) 2941–2953.
[3] R. Roesky, J. Weiguny, H. Bestgen, U. Dingerdissen, Appl. Catal. A Gen. 176 (1999) 213–220.
[4] X. Yong, F. Ping, Z. Baohua, G. Juan, Z. Lin, W. Xuehua, Mater. Lett. 123 (2014) 142–144.
[5] S.K. Sampath, J.F. Cordaro, J. Am. Ceram. Soc. 81 (1998) 649–654.
[6] G. Müller, Electroluminescence II. Semiconductors and Semimetals, Academic Press, New York, 2002.
[7] W. Strek, P.J. Dereń, A. Bednarkiewicz, M. Zawadzki, J. Wrzyszcz, J. Alloys Compd. 300 (2000) 456–458.
[8] M. Vrankić, B. Gržeta, V. Mandić, E. Tkalčec, S. Milošević, M. Čeh, B. Rakvin, J. Alloys Compd. 543 (2012) 213–220.
[9] P.J. Dereń, D. Stefańska, M. Ptak, M. Mączka, W. Walerczyk, G. Banach, J. Am. Ceram. Soc. 97 (2014) 1883–1889.
[10] H.StC. O'Neill, W.A. Dollase, Phys. Chem. Min. 20 (1994) 541–555.
[11] K.E. Sickafus, J.M. Wills, N.M. Grimes, J. Am. Ceram. Soc. 82 (1999) 3279–3292.
[12] R. Dovesi, R. Orlando, B. Civalleri, C. Roetti, V.R. Saunders, C.M. Zicovich-Wilson, Z. Krist. 220 (2005) 571–573.
[13] S.H. Vosko, L. Wilk, M. Nusair, Can. J. Phys. 58 (1980) 1200–1211.
[14] P.A.M. Dirac, Proc. Camb. Phil. Soc. 26 (1930) 376–385.
[15] M.F. Peintinger, D. Vilela Oliveira, T. Bredow, J. Comp. Chem. 34 (2013) 451–459.
[16] C. Gatti, V.R. Saunders, C. Roetti, J. Chem. Phys. 101 (1994) 10686–10696.
[17] W. Kohn, L.J. Sham, Phys. Rev. 140 (1965) A1133–A1138.
[18] J.P. Perdew, K. Burke, M. Ernzerhof, Phys. Rev. Lett. 77 (1996) 3865–3868.
[19] J.P. Perdew, K. Burke, M. Ernzerhof, Phys. Rev. Lett. 78 (1997) 1396–1399.
[20] J. Enkovaara, C. Rostgaard, J.J. Mortensen, J. Chen, M. Dulak, L. Ferrighi, J. Gavnholt, C. Glinsvad, V. Haikola, H.A. Hansen, H.H. Kristoffersen, M. Kuisma, A.H. Larsen, L. Lehtovaara, M. Ljungberg, O. Lopez-Acevedo, P.G. Moses, J. Ojanen, T. Olsen, V. Petzold, N.A. Romero, J. Stausholm-Møller, M. Strange, G.A. Tritsaris, M. Vanin, M. Walter, B. Hammer, H. Häkkinen, G.K.H. Madsen, R.M. Nieminen, J.K. Nørskov, M. Puska, T.T. Rantala, J. Schiøtz, S.R. Bahn, K.W. Jacobsen, J. Phys. Condens. Matter 22 (2010) 253202.
[21] S.R. Bahn, K.W. Jacobsen, Comput. Sci. Eng. 4 (2002) 56–66.
[22] D.F. Shanno, J. Optim. Theory Appl. Math. 25 (1978) 507–518.
[23] W.B. White, B.A. DeAngelis, Spectrochim. Acta 23A (1967) 985–995.
[24] http://www.cryst.ehu.es/rep/, 2016 (Accessed 27 April 2016).
[25] S.A. Hosseini, A. Niaei, D. Salari, S.R. Nabavi, Ceram. Int. 38 (2012) 1655–1661.
[26] A.V. Salker, S.M. Gurav, J. Mater. Sci. 35 (2000) 4713–4719.
[27] A. Chopelas, A.M. Hofmeister, Phys. Chem. Miner. 18 (1991) 279–293.
[28] R. Pandey, J.D. Gale, S.K. Sampath, J.M. Recio, J. Am. Ceram. Soc. 82 (1999) 3337–3341.
[29] http://nanochemistry.curtin.edu.au/local/docs/gulp/gulp4.0_manual.pdf, 2016 (Accessed 18 May 2016).
[30] MOLDRAW, a Program to Display and Manipulate Molecular and Crystalline Structures, 2016. http://www.moldraw.unito.it/_sgg/ (Accessed 04 October 2016).
[31] V. D'Ippolito, G.B. Andreozzi, D. Bersani, P.P. Lottici, J. Raman Spectrosc. 46 (2015) 1255–1264.
[32] S.K. Sampath, D.G. Kanhere, R. Pandey, J. Phys. Condens. Matter 11 (1999) 3635–3644.
[33] R. Khenata, M. Sahnoun, H. Baltache, M. Rérat, A.H. Reshak, Y. Al-Douri, B. Bouhafs, Phys. Lett. A 344 (2005) 271–279.
[34] F. Zerarga, A. Bouhemadou, R. Khenata, S. Binomran, Comput. Mater. Sci. 50 (2011) 2651–2657.
[35] H. Dixit, N. Tandon, S. Cottenier, R. Saniz, D. Lamoen, B. Partoens, V. Van Speybroeck, M. Waroquier, N. J. Phys. 13 (2011) 063002.
[36] H. Dixit, N. Tandon, S. Cottenier, R. Saniz, D. Lamoen, B. Partoens, Phys. Rev. B 87 (2013) 174101.
[37] C.M. Fang, C.-K. Loong, G.A. de Wijs, G. de With, Phys. Rev. B 66 (2002) 144301.
[38] S. Lopéz-Moreno, P. Rodriguez-Hernández, A. Muñoz, A.H. Romero, F.J. Manjon, D. Errandonea, E. Rusu, V.V. Ursaki, Ann. Phys. Berl. 523 (2011) 157–167.
[39] J.P. Perdew, Wang Yue, Phys. Rev. B 33 (1986) 8800–8802.
[40] V. Swamy, A. Kuznetsov, L.S. Dubrovinsky, R.A. Caruso, D.G. Shchukin, B.C. Muddle, Phys. Rev. B 71 (2005) 184302.
[41] N. Aaron Deskin, M. Dupuis, Phys. Rev. B 75 (2007) 195217.
[42] P. Calvani, Riv. Nuovo Cimento 24 (2001) 1–71.
[43] D. Emin, Polarons, Cambridge University press, 2013.
[44] A. Mortensen, D.H. Christensen, O. Faurskov Nielsen, J. Raman Spectrosc. 22 (1991) 47–49.